

Three-Dimensional Pt-on-Pd Bimetallic Nanodendrites Supported on Graphene Nanosheet: Facile Synthesis and Used as an Advanced Nanoelectrocatalyst for Methanol Oxidation

Shaojun Guo, Shaojun Dong, and Erkang Wang*

State Key Laboratory of Electroanalytical Chemistry, Changchun Institute of Applied Chemistry, Chinese Academy of Sciences, Changchun 130022, Jilin, China, and Graduate School of the Chinese Academy of Sciences, Beijing 100039, China

Synthesis of Pt nanocrystals (NCs) with controlled sizes and shapes is one of the most attractive goals in developing highly active Pt catalysts for many types of industrial reactions such as fuel cell reactions, CO oxidation in a catalytic converter, nitric acid production, and petroleum cracking, etc.^{1–3} Effectively controlling the morphology of Pt nanostructures can provide a great opportunity to improve their catalytic properties and increase their activity on a mass or specific basis.³ Inspired by this intention, a variety of chemical protocols have been developed for achieving partial control of NC shapes in a cube,^{4,5} tube,^{6,7} wire,^{8–11} tetrahedahedral Pt,¹² mesoporous nanostructure,^{13–16} and dendrite,^{17–20} among which Pt nanodendrites are of particular interest in catalysis due to their porous structure, high surface area, and high catalytic activity. For instance, Yamauchi *et al.*¹⁹ reported that dendritic NCs could be synthesized in high yield *via* a block-copolymer-mediated reduction process. The as-prepared dendritic NPs gave a surface area of $56\text{ m}^2\text{ g}^{-1}$, which is the highest for unsupported Pt materials. Therefore, using Pt-based nanodendrite as a catalyst, one would expect that less Pt is needed in the fuel cell reactions, a goal that has long been sought for commercialization of the fuel cell technology.

On the other hand, hybridization provides an effective strategy for enhancing the functionality of materials.²¹ In order to further maximize the activity of Pt and minimize the use of previous Pt, it is very necessary to load Pt nanostructures with

ABSTRACT Graphene nanosheet, the hottest material in physics and materials science, has been studied extensively because of its unique electronic, thermal, mechanical, and chemical properties arising from its strictly 2D structure and because of its potential technical applications. Particularly, these remarkable characteristics enable it to be a promising candidate as a new 2D support to load metal nanoparticles (NPs) for application in fuel cells. However, constructing high-quality graphene/bimetallic NP hybrids with high electrochemical surface area (ECSA) remains a great challenge to date. In this paper, we demonstrate for the first time a wet-chemical approach for the synthesis of high-quality three-dimensional (3D) Pt-on-Pd bimetallic nanodendrites supported on graphene nanosheets (TP-BNGN), which represents a new type of graphene/metal heterostructure. The resulting hybrids were characterized by atomic force microscopy (AFM), transmission electron microscopy (TEM), high-resolution TEM (HRTEM), energy-dispersive X-ray (EDX) spectroscopy, X-ray photoelectron spectroscopy (XPS), thermogravimetric analysis (TGA), Raman spectroscopy, and electrochemical technique. It is found that small single-crystal Pt nanobranches supported on Pd NCs with porous structure and good dispersion were directly grown onto the surface of graphene nanosheets, which exhibits high electrochemical active area. Furthermore, the number of nanobranches for Pt-on-Pd bimetallic nanodendrites on the surface of graphene nanosheets could be easily controlled *via* simply changing the synthetic parameters, thus resulting in the tunable catalytic properties. Most importantly, the electrochemical data indicate that the as-prepared graphene/bimetallic nanodendrite hybrids exhibited much higher electrocatalytic activity toward methanol oxidation reaction than the platinum black (PB) and commercial E-TEK Pt/C catalysts.

KEYWORDS: graphene nanosheet · bimetallic nanostructure · nanodendrite · nanoelectrocatalyst · fuel cell

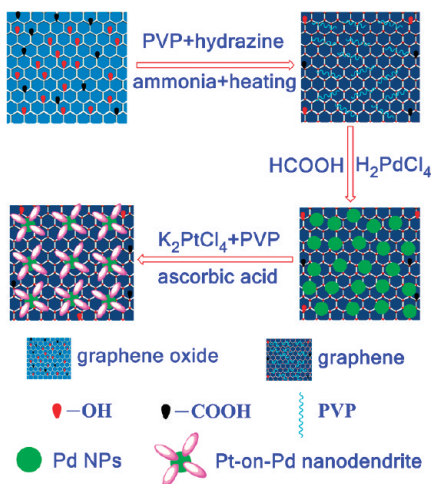
high activity on the surface of supporting nanomaterials with low cost, high surface area, and good electrical conductivity, which not only maximize the availability of nanosized electrocatalyst surface area for electron transfer but also provide better mass transport of reactants to the electrocatalyst. The recent emergence of graphene nanosheets has opened a new avenue for utilizing 2D new carbon material as a support because of its high conductivity (10^3 – 10^4 S/m), huge surface area

*Address correspondence to ekwang@ciac.jl.cn.

Received for review October 21, 2009 and accepted December 2, 2009.

Published online December 15, 2009. [10.1021/nm9014483](https://doi.org/10.1021/nm9014483)

© 2010 American Chemical Society



Scheme 1. Procedure to design graphene nanosheet/Pt-on-Pd bimetallic nanodendrite hybrids.

(calculated value, $2630 \text{ m}^2/\text{g}$), unique graphitized basal plane structure, and potential low manufacturing cost.^{22–24} The integration of graphene and certain functional particles (such as Pt NCs) presents special features in the new hybrids, useful, for example, in optics, electronics, catalysis, sensors, and so on. However, only a few examples^{25–27} of the synthesis of graphene/Pt hybrids have been demonstrated to date, in which the obtained Pt NPs have relatively wide size range on the surface of graphene, and particularly, the surface area of the obtained hybrids is relatively low. In addition, bimetallic NPs have been attracting more and more attention due to their enhanced catalytic properties relative to individual NPs.^{28–34} For instance, Au/Pt bimetallic NPs could significantly increase the surface area of Pt, which is an essential factor in improving the catalytic activity of Pt.^{29,30} Therefore, the synthesis of a new type of high-quality graphene nanosheet/3D bimetallic nanodendrite hybrids (combining the advantages of graphene nanosheet and bimetallic nanodendrite) with high surface area as a high-efficiency nanoelectrocatalyst is highly desirable and technologically important.

In this paper, we demonstrate for the first time a wet-chemical approach for the synthesis of high-quality

three-dimensional (3D) Pt-on-Pd bimetallic nanodendrites supported on graphene nanosheets (TP-BNGN), which represents a new type of graphene/metal heterostructure with several important benefits. (a) Small single-crystal Pt nanobranches supported on Pd NCs with porous structure and good dispersion were directly grown onto the surface of graphene nanosheets. The corresponding hybrids exhibit high electrochemical active area ($81.6 \text{ m}^2/\text{g}$). (b) The number of branches for Pt-on-Pd bimetallic nanodendrite on the surface of graphene nanosheets could be easily controlled via simply changing the synthetic parameters, thus resulting in the tunable catalytic properties. (c) The as-prepared graphene/bimetallic nanodendrite hybrids exhibited much higher electrocatalytic activity toward methanol oxidation reaction than the platinum black (PB) and commercial E-TEK Pt/C catalysts.

RESULTS AND DISCUSSION

The whole preparation strategy for constructing the TP-BNGN is shown in Scheme 1 (for detailed experimental steps, please see Experimental Section). In the first step, a simple wet-chemical route was employed for preparing poly(*N*-vinyl-2-pyrrolidone) (PVP)-functionalized graphene nanosheets through the heating reduction of graphene oxide in the presence of hydrazine. Figure 1A shows the typical atomic force microscopic (AFM) image of PVP-functionalized graphene nanosheets. It is observed that the mica substrate is covered with a number of nanosheets with high purity. The corresponding cross-sectional view (Figure S1A, Supporting Information) of the typical AFM image of graphene nanosheets (Figure 1A) indicates that the average thickness of nanosheets is about 2 nm. It should be noted that the colloidal suspensions of graphene sheets decorated by PVP show high stability in water, ethanol, and dimethylformamide (data not shown), which can be ascribed to the strong $\pi-\pi$ interactions between graphene and PVP molecules.³¹ In the second step, PVP-functionalized graphene nanosheets were used to load small Pd nanoparticles (NPs) for pro-

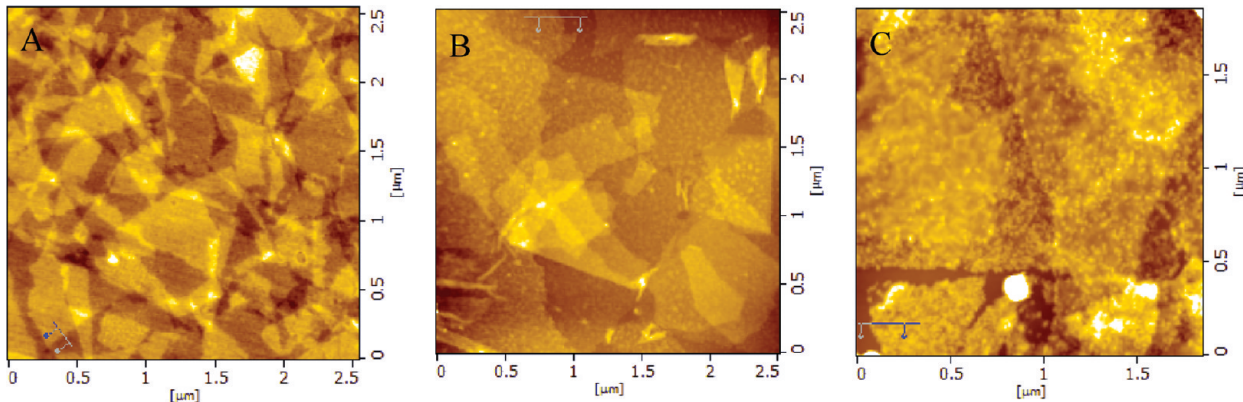


Figure 1. AFM images of PVP-functionalized graphene nanosheets (A), graphene/Pd NC hybrids (B), and graphene/bimetallic nanodendrite hybrids (C).

ducing graphene/Pd NP hybrids *via* a simple and surfactantless route at room temperature. Figure 1B shows the AFM image of graphene/Pd NP hybrids. The result shows that the as-obtained hybrids have a rougher surface than the pristine graphene nanosheets (Figure 1A), indicating Pd NPs were facilely adsorbed on the surface of graphene nanosheets (Figure S1B). The transmission electron microscopy (TEM) images of the as-prepared graphene/Pd NP hybrids are shown in Figure 2. It is observed that small Pd NPs supported on the surface of graphene nanosheets have a size of about 3 nm (Figure 2B). The high-resolution TEM (HRTEM) images (Figure 2C) of Pd NPs indicate that they are single crystal with many (111) facets. In the third step, single-crystal Pd NCs supported on graphene nanosheets were used as seeds to direct the dendritic growth of Pt upon the reduction of K_2PtCl_4 by ascorbic acid in an aqueous solution. Figure 1C shows the AFM image of TP-BNGN (sample 1). The result indicates that the as-obtained hybrids have a much rougher surface (the corresponding cross-sectional view of Figure 1C is shown in Figure S1C) than the graphene/Pd NPs hybrids (Figure 1B), indicating that Pt has grown onto the surface of Pd NPs (Pd and Pt have a lattice mismatch of only 0.77%).²⁰ Typical TEM images (Figure 3A–C) of the product revealed that several Pt branches had grown from a Pd core into dendritic tendrils. The Pt-on-Pt bimetallic nanodendrites had an average size of 15 nm. In order to further reveal the detailed structure of Pt-on-Pd nanodendrites, HRTEM images of typical nanodendrites are shown in Figure 3D,E and Figure S2, which clearly show overgrowth of Pt branches at multiple sites on the Pd seed (Pt and Pd have contrast difference with a darker Pd center surrounded by several lighter branches in the nanodendrites).

For the Pt branches, the diameter was 3–5 nm. HRTEM image of individual Pt branches (circled part, Figure 3E or the corresponding part in Figure S2B) shows their single-crystalline structure with highly ordered,

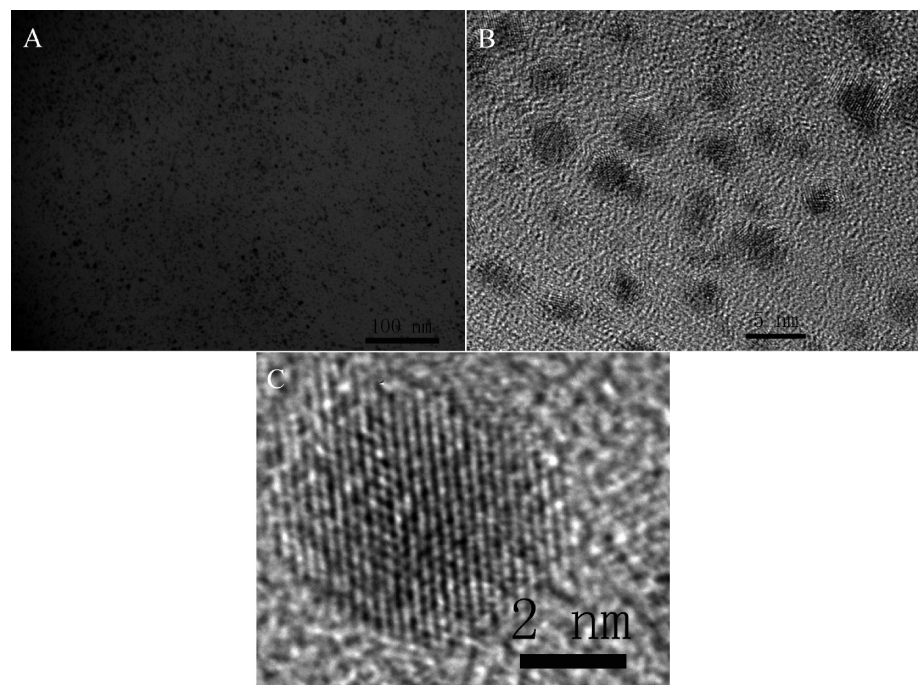


Figure 2. TEM (A) and HRTEM (B,C) images of graphene/Pd NP hybrids. Reaction conditions: 500 μ L of graphene solution and 250 μ L of 56.4 mM H_2PdCl_4 .

continuous fringe patterns. The measured interplanar spacing for the lattice fringes is 0.23 nm, which corresponds to the (111) lattice plane of face-centered cubic (fcc) Pt. While the fast Fourier transform (FFT) pattern (Figure 3F) of the HRTEM image (circled part, Figure 3E) further indicates that the Pt nanobranch is a single crystal.

The formation of TP-BNGN was further characterized by energy-dispersive X-ray (EDX) spectroscopy (Figure 4A), X-ray photoelectron spectroscopy (XPS, Figure 4B–E), thermogravimetric analysis (TGA, Figure 5), and Raman spectroscopy (Figure 6). The corresponding EDX spectrum (Figure 4A) of TP-BNGN shows the peaks corresponding to C, N, Pd, and Pt elements, confirming the existence of bimetallic Pd–Pt NPs on the surface of PVP-functionalized graphene nanosheets.

continuous fringe patterns. The measured interplanar spacing for the lattice fringes is 0.23 nm, which corresponds to the (111) lattice plane of face-centered cubic (fcc) Pt. While the fast Fourier transform (FFT) pattern (Figure 3F) of the HRTEM image (circled part, Figure 3E) further indicates that the Pt nanobranch is a single crystal.

The formation of TP-BNGN was further characterized by energy-dispersive X-ray (EDX) spectroscopy (Figure 4A), X-ray photoelectron spectroscopy (XPS, Figure 4B–E), thermogravimetric analysis (TGA, Figure 5), and Raman spectroscopy (Figure 6). The corresponding EDX spectrum (Figure 4A) of TP-BNGN shows the peaks corresponding to C, N, Pd, and Pt elements, confirming the existence of bimetallic Pd–Pt NPs on the surface of PVP-functionalized graphene nanosheets.

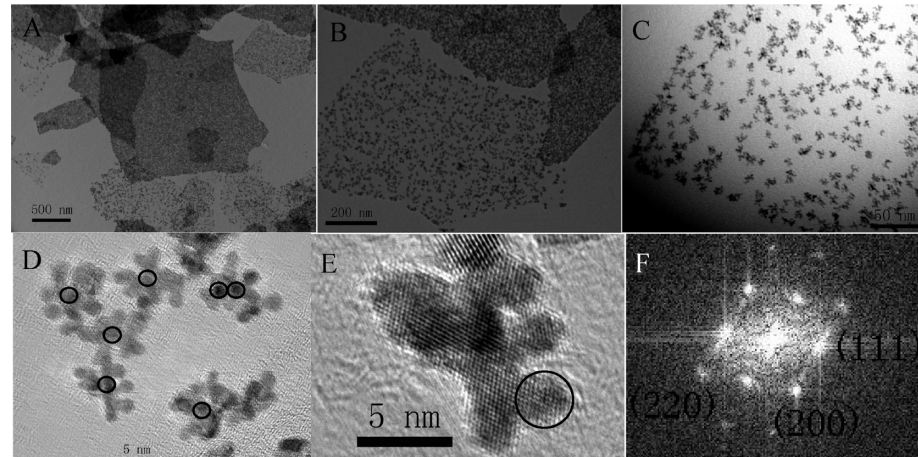


Figure 3. TEM (A–C) and HRTEM (D,E) images of TP-BNGN at different magnifications. The circled parts in panel D denote Pd NPs. FFT pattern (F) of the HRTEM image shown in panel E (circled part).

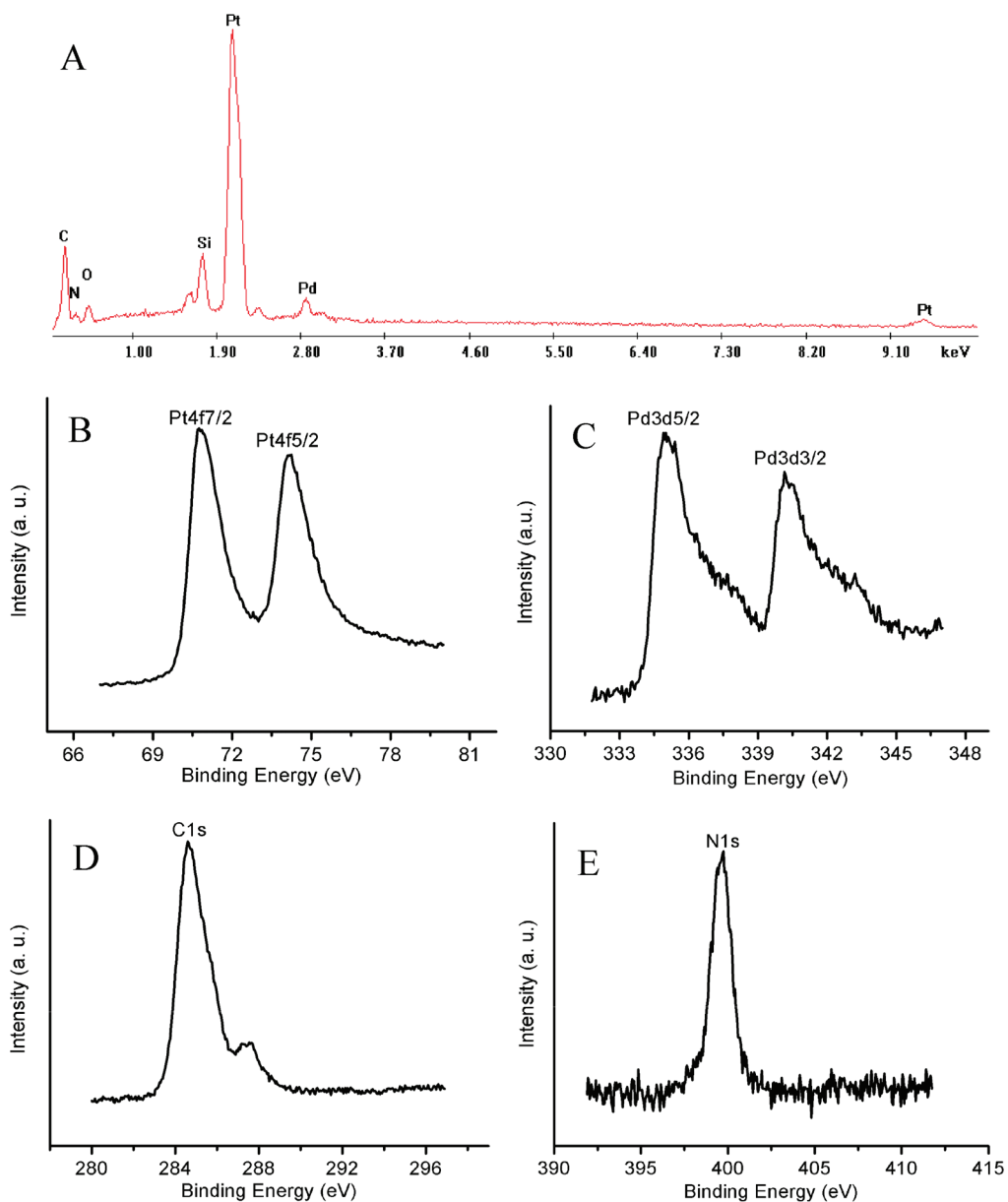


Figure 4. EDX (A) and XPS (B–E) patterns of TP-BNGN: (B) Pt, (C) Pd, (D) C, (E) N.

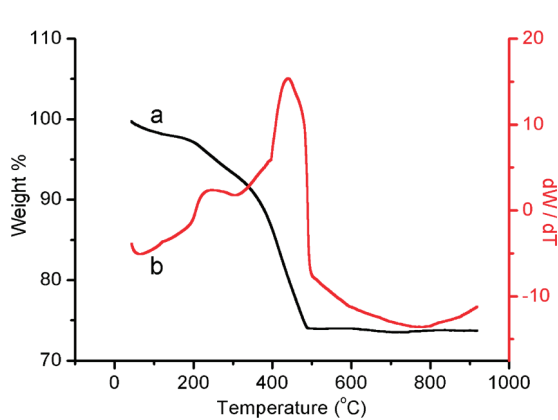


Figure 5. TGA of TP-BNGN. The black line (a) shows the change in weight, while the red line (b) shows the derivative of the change in weight with respect to temperature.

Furthermore, XPS patterns of the resulting TP-BNGN show significant Pt4f signals corresponding to the bind-

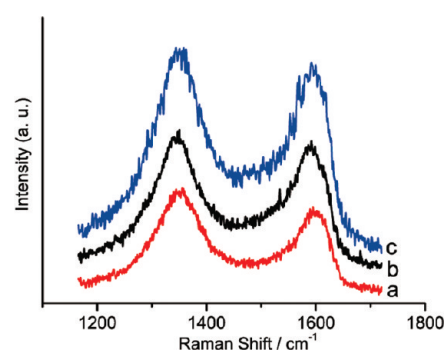


Figure 6. Raman spectroscopy of graphene nanosheet (trace a) prepared according to ref 36, PVP-functionalized graphene (trace b) and TP-BNGN (trace c).

ing energy of Pt (Figure 4B), significant Pd4f signals corresponding to the binding energy of Pd (Figure 4C), significant C signal corresponding to the binding energy of C (Figure 4D), and N signal (Figure 4E) corresponding to the binding energy of N (originate from polymer, PVP), which further support the conclusion that bimetallic Pd–Pt NPs have been effectively assembled on the surface of PVP-functionalized graphene

nanosheets. TGA of TP-BNGN, as shown in Figure 5, displays the weight loss of sample 1 (trace a in Figure 5) and the corresponding derivative of the weight loss with respect to temperature (trace b in Figure 5). The derivative peak seen at temperatures of ~ 230 °C could be ascribed to the decomposition of the polymer, PVP.³⁵ The derivative peak at ~ 420 °C exhibiting large loss of weight could be attributed to the oxidation of graphene nanosheets. The above TGA result further supports the conclusion that TP-BNGNs have been facilely obtained. In addition, whether the structural changes occurred during the chemical processing from graphene³⁶ to PVP-functionalized graphene, and then to TP-BNGN or not, is reflected in their Raman spectra (Figure 6). The peaks at 1348 and 1585 cm⁻¹ could be ascribed to the D and G bands of graphene, respectively.^{37,38} The D band corresponds to defects in the curved graphene sheet, and staging disorder, while the G band is related to the graphitic hexagon-pinch mode. It is found that after functionalization with PVP, and even bimetallic nanodendrite, the D/G intensity ratio did not change obviously, suggesting that the functionalization of graphene nanosheets did not reduce the size of in-plane sp² domains greatly (determining the electrical conductivity of graphene nanosheets). It should be noted that the as-obtained TP-BNGN has high stability (the nanodendrites will not fall off when sonicking the TP-BNGN solution), which could be ascribed to the strong coordination interaction between poly(*N*-vinyl-2-pyrrolidone) (PVP, existing on the surface of graphene) and nanodendrites.^{8–11}

We have attempted to synthesize Pt nanodendrites supported graphene nanosheets in the absence of Pd NPs, but it failed; only foam-like Pt nanospheres with sizes of 20–80 nm supported on

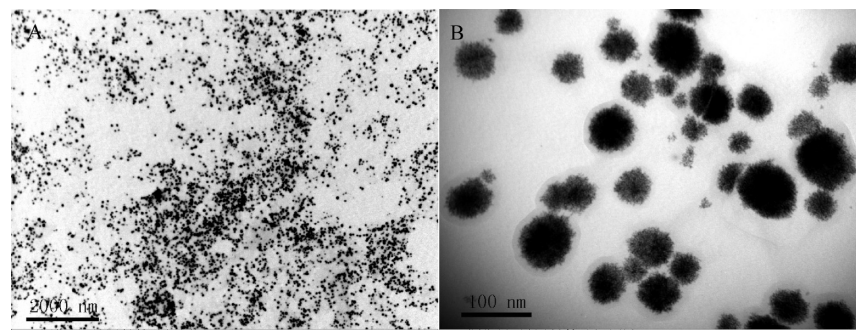


Figure 7. TEM images of graphene/Pt nanosphere hybrids in the absence of Pd seeds at different magnifications.

graphene nanosheets were obtained (Figure 7), indicating that Pd seeds play an important role in constructing the dendritic nanostructure here. The observed dendritic growth of Pt branches can probably be attributed to the high-rate reduction and (111) facet epitaxial growth of Pt as mediated by Pd seeds with many (111) facets, which is in accordance with the previous report²⁰ and HRTEM results (the nucleation sites for Pt appear to be distributed over the entire surface of Pd seed, as shown in Figure S2 of the Supporting Information). It is interestingly found that the number of Pt branches on nanodendrites (supported on graphene nanosheets) could be easily controlled *via* simply changing reaction parameters. For instance, bimetallic nanodendrites with more Pt nanobranches (low concentration of graphene leads to relatively low amounts of Pd NPs adsorbed on the surface of graphene nanosheets) are effectively supported on the surface of graphene nanosheets (sample 2) when 250 μL of graphene aqueous solution was added into the mixture (Figure 8) under identical conditions used for prepara-

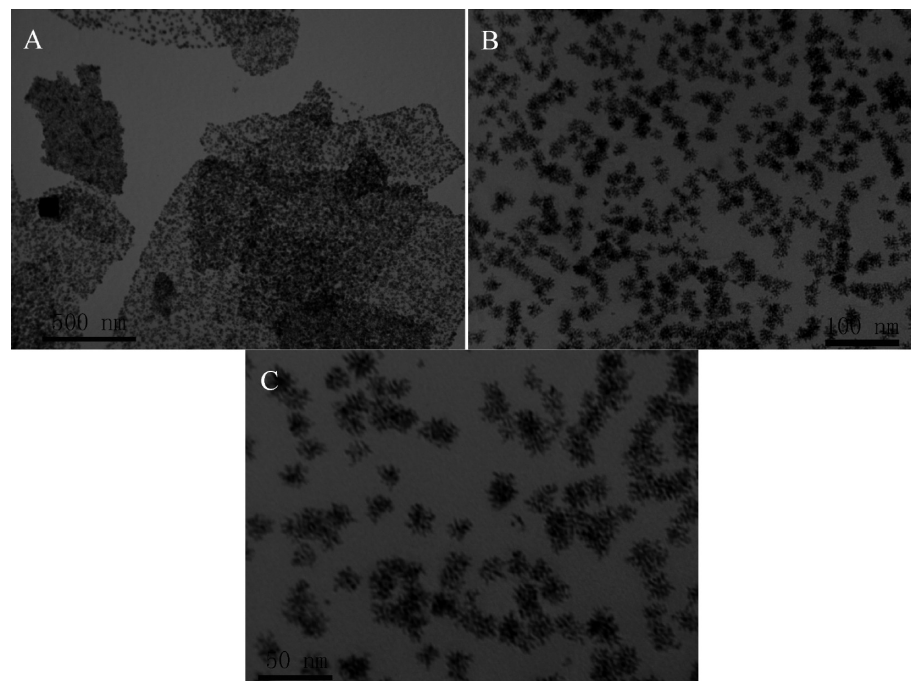


Figure 8. TEM images of TP-BNGN (sample 2) at different magnifications. Reaction conditions: 250 μL of graphene solution, 250 μL of PVP (1 M), and 0.5 mL of K₂PtCl₄ (0.1 M).

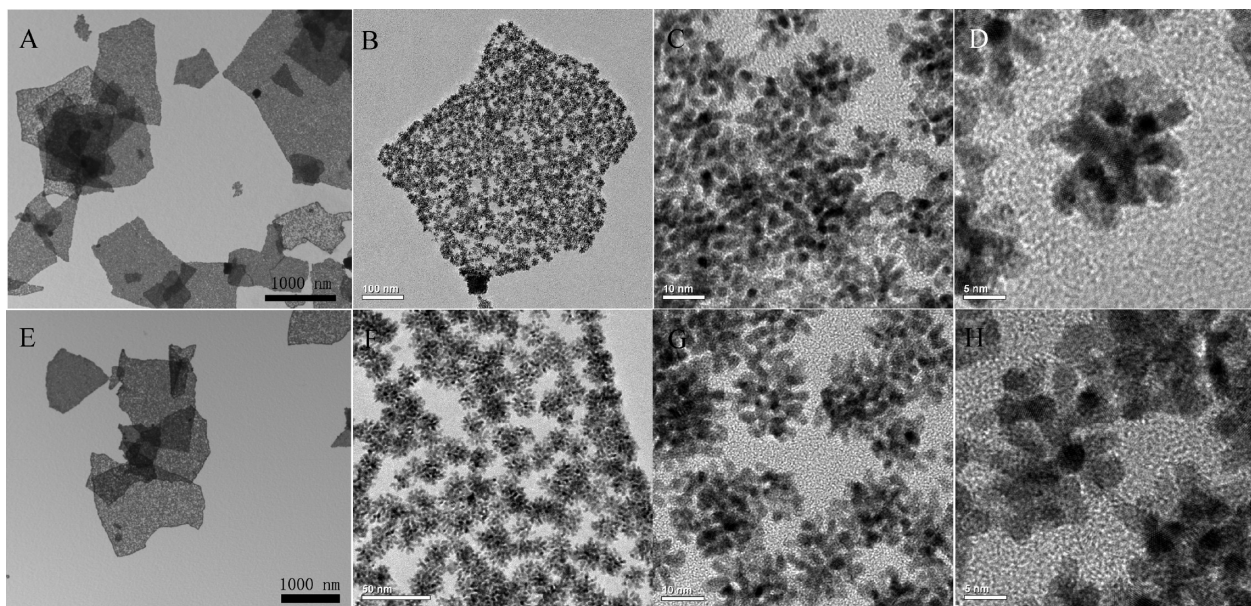


Figure 9. TEM images (A–D) of TP-BNGN (sample 3) at different magnifications. Reaction conditions: 500 μ L of graphene solution, 500 μ L of PVP (1 M), and 1 mL of K_2PtCl_4 (0.1 M). TEM images (E–H) of TP-BNGN (sample 4) at different magnifications. Reaction conditions: 500 μ L of graphene solution, 750 μ L of PVP (1 M), and 1.5 mL of K_2PtCl_4 (0.1 M).

ing sample 1. When increasing the amounts of Pt precursor to 1 mL (sample 3) and 1.5 mL (sample 4) under identical conditions used for preparing sample 1, the density of Pt nanobranches can further increase, as shown in Figure 9A–D and Figure 9E–H, respectively. Thus, the electrocatalytic activity of TP-BNGN can be facilely tuned by changing the above reaction parameters.

Inspired by their attractive structure and special property (high solubility in water, Figure S3 in the

Supporting Information), the TP-BNGNs were tested as nanoelectrocatalysts for studying their catalytic activity. By using hydrogen adsorption–desorption methods in conjunction with cyclic voltammetry (CV), the ECSA of TP-BNGN, E-TEK Pt/C, and platinum black (PB) catalysts were measured (see Figure 10A and Table 1). It is found that the ECSA value of TP-BNGN ($81.6 \text{ m}^2/\text{g}$) is higher than those of E-TEK catalyst ($54.7 \text{ m}^2/\text{g}$), PB ($19.2 \text{ m}^2/\text{g}$), graphene/Pt NP hybrids ($44.6 \text{ m}^2/\text{g}$),²⁶ and re-

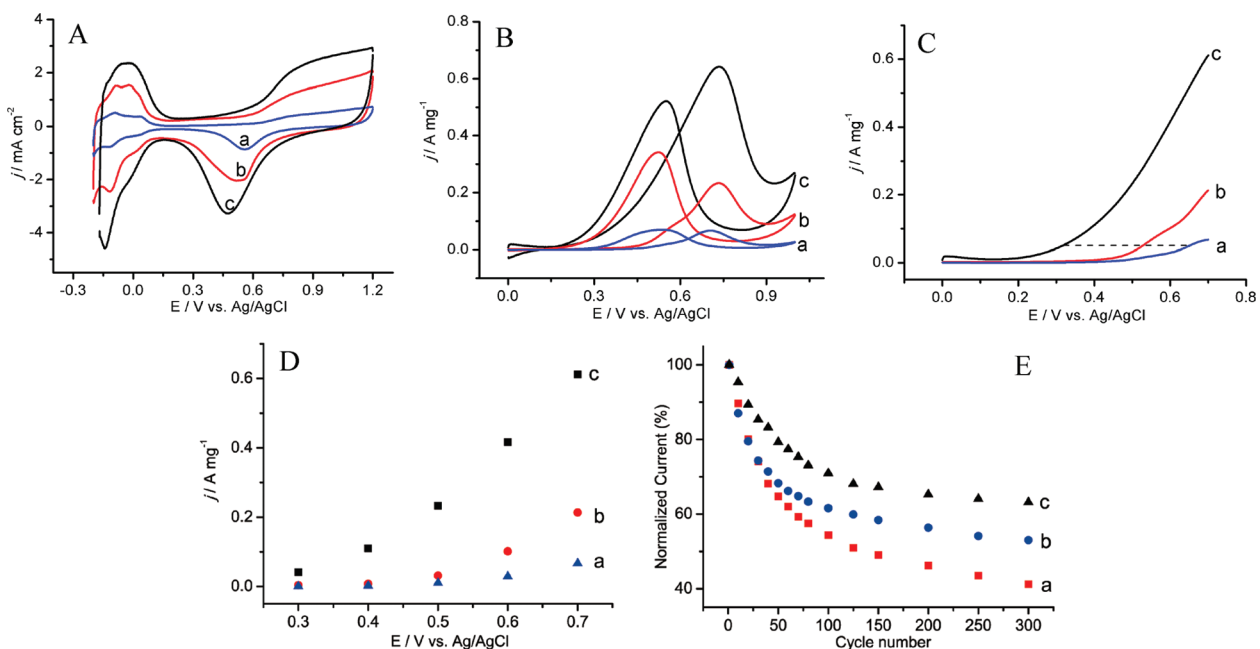


Figure 10. (A) CVs of PB (trace a), E-TEK catalyst (trace b), and TP-BNGN (trace c) modified GC electrodes in a N_2 -sparged 0.5 M H_2SO_4 solution at the scan rate of 20 mV/s. CVs (B) and linear sweep voltammetry (C) of PB (trace a), E-TEK catalyst (trace b), and TP-BNGN (trace c) modified GC electrodes in a 0.5 M H_2SO_4 solution containing 1 M methanol at the scan rate of 50 mV/s. (D) Potential-dependent current density of methanol electrooxidation on the PB catalyst (a), E-TEK catalyst (b), and TP-BNGN (c). (E) Electrocatalytic cycling stability of E-TEK catalyst (curve a), PB (curve b), and TP-BNGN (curve c). All of the above data were normalized to the peak current of first cycle.

TABLE 1. Catalyst Characterization and Catalytic Performance Characteristics of Different Graphene/Pt-on-Pd Bimetallic Nanodendrite Hybrids, E-TEK Catalyst, and Platinum Black

catalyst	sample 1	sample 2	sample 3	sample 4	E-TEK	platinum black
$A_{\text{Pt}} (\text{m}^2/\text{g}_{\text{Pt}})$	81.6	72.0	68.1	63.4	54.7	19.2
$i_{\text{m-peak}} (\text{mA}/\text{mg}_{\text{Pt}})^a$	647.2	582.7	538.6	486.5	239.9	70.8

^aMass activities, $i_{\text{m-peak}}$, determined at the peak potential and in the condition of 0.5 M H₂SO₄ solution containing 1 M methanol.

cent state-of-art Pt-based nanomaterials such as Pd–Pt bimetallic nanodendrite (57.1 m²/g),²⁰ carbon nanotube (CNT)/ionic liquid/Pt NP hybrids (71.4 m²/g),³⁹ mesoporous Pt with giant mesocage (74 m²/g),¹³ and dendritic Pt NPs (56 m²/g),¹⁹ etc., most likely a result of the particular structure of bimetallic nanodendrites and their better dispersion on the graphene nanosheets with high surface area. This result also reveals that the TP-BNGNs are electrochemically more accessible, which is very important for the electrocatalytic reactions.

Methanol was selected as a model molecule for studying the electrocatalytic performance of TP-BNGN. Figure 10B,C shows the CVs (B) and linear sweep voltammetry (C) of PB (trace a), E-TEK catalyst (trace b), and TP-BNGN (trace c) modified glassy carbon (GC) electrodes in a 0.5 M H₂SO₄ solution containing 1 M methanol. The mass current density for CH₃OH oxidation in TP-BNGN (Figure 10B) was found to be about 3.0 and 9.5 higher than those of E-TEK and PB catalysts, respectively. It should be noted that the mass activity of TP-BNGN (Figure 10B, line c) is also higher than those of recent state-of-art Pt-based nanomaterials such as carbon nanofibers or CNT-supported Pt NPs,⁴⁰ CNTs/ionic liquid/Pt NPs hybrids,³⁹ CNT/Pt composite catalysts,^{41,42} polyaniline/Pt NPs hybrid,⁴³ and graphene/Pt NPs hybrids,²⁶ etc. (indexing 1 M methanol). Furthermore, as indicated by dashed lines in Figure 10C, the corresponding potential on TP-BNGN is much lower than that on E-TEK or PB catalyst at a given oxidation current density. It means that TP-BNGN exhibited better performance for methanol electrooxidation than the E-TEK and PB catalysts at all applied potential (from 0.3 to 0.7 V), as shown in Figure 10D. Thus, all of the above data reveal that the TP-BNGNs exhibit much enhanced catalytic activity for MOR. It is worthwhile to say that higher activity in

electrochemical performance observed here can probably be attributed to three major factors: (i) The size of Pt nanobranches is small (Pt NPs with small and proper size own higher electroactivity than that with big size), which is comparable to commercial nanocatalysts;²⁰ (ii) The bimetallic dendritic NPs could provide high ECSA, thus leading to high electrocatalytic activity. (iii) Better dispersion of dendritic NPs on the graphene nanosheets with high surface area should be also emphasized. Furthermore, more detailed data comparisons for different hybrids, E-TEK and PB, such as ECSA, Pt surface area of the catalyst (A_{Pt}) and mass activity, etc., are shown in Table 1. It is found that bimetallic nanodendrites with proper branched degrees supported on graphene nanosheets have the highest electrocatalytic activity.

In addition, the ratio of the forward oxidation current peak (I_f) to the reverse current peak (I_b), I_f/I_b , is an important index of the catalyst tolerance to the poisoning species, Pt=C=O.^{40–42} A higher ratio indicates more effective removal of the poisoning species on the catalyst surface. As shown in Figure 10B, the I_f/I_b ratio of TP-BNGN is 1.25, which is higher than those of the PB (0.95) and E-TEK catalysts (0.70), showing better catalyst tolerance of TP-BNGN. The electrocatalytic cycling stabilities of the TP-BNGN and commercial catalysts in 1 M CH₃OH + 0.5 M H₂SO₄ solution have also been compared by using CV cycling, as shown in Figure 10E. It can be seen that the loss of the electrocatalytic activity for TP-BNGN is lower than those of E-TEK and PB catalysts, further indicating that the present TP-BNGN has good stability.

CONCLUSIONS

In summary, we have developed a facile wet-chemical procedure to synthesize graphene nanosheet/3D Pt-on-Pd bimetallic nanodendrite hybrids using 2D graphene nanosheet as a support. The bimetallic nanodendrites with controllable size or different numbers of Pt branches adhere to graphene nanosheets, which exhibit an enlarged ECSA. Most importantly, the present study shows that TP-BNGNs have a much higher catalytic activity than conventional E-TEK Pt/C and PB electrocatalysts for methanol electrooxidation, demonstrating a new and powerful approach for the development of high-performance Pt-based electrocatalysts for fuel cells.

EXPERIMENTAL SECTION

Materials: Poly(N-vinyl-2-pyrrolidone) (PVP · K30, molecular weight = 30 000–40 000), PdCl₂, H₂SO₄, HCOOH, ascorbic acid (AA), and ethanol were purchased from the Shanghai Chemical Factory (Shanghai, China) and used as received without further purification. Graphite and K₂PtCl₄ were purchased from Alfa Aesar. Water used throughout all experiments was purified with the Millipore system.

Apparatus: TEM measurements were made on a HITACHI H-8100 EM with an accelerating voltage of 200 kV. HRTEM im-

ages were obtained with a JEM-2100F high-resolution transmission electron microscope operating at 200 kV. Thermogravimetric analysis (TGA) of sample was performed on a Pyris Diamond TG/DTA thermogravimetric analyzer (Perkin-Elmer Thermal Analysis). Sample was heated under an air atmosphere from room temperature to 900 at 10 °C/min⁻¹. XPS measurement was performed on an ESCALAB-MKII spectrometer (VG Co., United Kingdom) with Al K α X-ray radiation as the X-ray source for excitation. AFM image was taken by using a SPI3800N microscope (Seiko Instruments, Inc.) operating in the tapping mode with

standard silicon nitride tips. Typically, the surface was scanned at 1 Hz with the resolution of 256 lines/image. Raman spectra were obtained on a J-Y T64000 Raman spectrometer using an Olympus microscope and a 50 \times long working distance objective to focus the laser beam onto a spot of about 1 μm^2 . The Raman band of a silicon wafer at 520 cm^{-1} was used to calibrate the spectrometer. The composition of TP-BNGN was determined by inductively coupled plasma mass spectroscopy (ICP-MS, X Series 2, Thermo Scientific USA). CV experiments were performed with a CHI 832 electrochemical analyzer (CH Instruments, Chenzhua Co., Shanghai, China). A conventional three-electrode cell was used, including a Ag/AgCl (saturated KCl) electrode as reference electrode, a platinum wire as counter electrode, and modified GC as working electrode.

Preparation of PVP-Functionalized Graphene: First, the graphite oxide was synthesized from natural graphite powder according to the literature.³⁶ Then, exfoliation of graphite oxide to graphene oxide (GO) was achieved by ultrasonication of the dispersion for 40 min (1000 W, 20% amplitude). Finally, a homogeneous GO aqueous dispersion (0.5 mg/mL) was obtained. In a typical procedure for chemical conversion of graphene oxide to PVP-functionalized graphene, 400 mg of PVP was added into 100 mL of homogeneous GO dispersion (0.25 mg/mL), followed by stirring for 12 h. Then, to the resulting dispersion were added 35 μL of hydrazine solution (>50% w/w) and 400 μL of ammonia solution (25% w/w). After being vigorously shaken or stirred for a few minutes, the mixture was stirred for 1 h at 95 °C. Finally, the stable black dispersion was centrifuged one time and dissolved in 12.5 mL of water (completely derived from 25 mg of GO).

Preparation of Graphene Nanosheet/Pd NP Hybrids: Amounts of 250 and 500 μL of PVP-functionalized graphene aqueous solution were dissolved with water (the final total volume of water is 1.5 mL), followed by the addition of 250 μL of H₂PdCl₆ (56.4 mM) and 0.35 mL of HCOOH. The mixture was stored at room temperature until the Pd precursor was reduced completely. Then, the solution was centrifuged and washed several times with double-distilled water and dissolved in 3.8 mL of water.

Preparation of Graphene Nanosheet/Pt-on-Pd Bimetallic Nanodendrite Hybrids: The as-prepared suspension of graphene/Pd NP hybrids (3.8 mL), 250 μL of PVP aqueous solution (1 M), and 1.45 mL of ascorbic acid (AA) aqueous solution (0.2 M) were added into a 10 mL flask. The mixture was heated to 90 °C in air under magnetic stirring. Meanwhile, 0.5 mL of K₂PtCl₆ aqueous solution (0.1 M) was then rapidly injected into the flask by pipet. The reaction mixture was heated at 90 °C in air for 3 h and then cooled to room temperature. The product was collected by centrifugation and washed several times with water for further electrochemical measurements.

Electrocatalytic Experiment: Prior to the surface coating, the GC electrode was polished carefully with 1.0, 0.3, and 0.05 μm alumina powder and rinsed with deionized water, followed by sonication in acetone and doubly distilled water successively. Then, the electrode was allowed to dry under nitrogen. For MOR, 5 μL of graphene nanosheet/bimetallic nanodendrite hybrid or E-TEK catalyst or PB solution was dropped on the surface of the GC electrode and dried with an infrared lamp. Then, 5 μL of Nafion (0.2%) was placed on the surface of the above material modified GC electrode and dried before electrochemical experiments.

Acknowledgment. This work was supported by the National Natural Science Foundation of China (No. 20820102037) and the 973 Project (Nos. 2009CB930100 and 2010CB933600).

Supporting Information Available: Figures S1–S3. This material is available free of charge via the Internet at <http://pubs.acs.org>.

REFERENCES AND NOTES

- Diezi, S.; Ferri, D.; Vargas, A.; Mallat, T.; Baiker, A. The Origin of Chemo- and Enantioselectivity in the Hydrogenation of Diketones on Platinum. *J. Am. Chem. Soc.* **2006**, *128*, 4048–4057.
- Chen, J.; Lim, B.; Lee, E. P.; Xia, Y. N. Shape-Controlled Synthesis of Platinum Nanocrystals for Catalytic and Electrocatalytic Applications. *Nano Today* **2009**, *4*, 81–95.
- Tian, N.; Zhou, Z.-Y.; Sun, S.-G. Platinum Metal Catalysts of High-Index Surfaces: From Single-Crystal Planes to Electrochemically Shape-Controlled Nanoparticles. *J. Phys. Chem. C* **2008**, *112*, 19801–19817.
- Wang, C.; Daimon, H.; Lee, Y.; Kim, J.; Sun, S. Synthesis of Monodisperse Pt Nanocubes and Their Enhanced Catalysis for Oxygen Reduction. *J. Am. Chem. Soc.* **2007**, *129*, 6974–6975.
- Wang, C.; Daimon, H.; Onodera, T.; Koda, T.; Sun, S. A General Approach to the Size- and Shape-Controlled Synthesis of Platinum Nanoparticles and Their Catalytic Reduction of Oxygen. *Angew. Chem., Int. Ed.* **2008**, *47*, 3588–3591.
- Chen, Z.; Waje, M.; Li, W.; Yan, Y. Supportless Pt and PtPd Nanotubes as Electrocatalysts for Oxygen-Reduction Reactions. *Angew. Chem., Int. Ed.* **2007**, *46*, 4060–4063.
- Guo, S. J.; Dong, S. J.; Wang, E. K. A General Method for the Rapid Synthesis of Hollow Metallic or Bimetallic Nanoelectrocatalysts with Urchinlike Morphology. *Chem.—Eur. J.* **2008**, *14*, 4689–4695.
- Chen, J.; Herricks, T.; Geissler, M.; Xia, Y. Single-Crystal Nanowires of Platinum Can Be Synthesized by Controlling the Reaction Rate of a Polyol Process. *J. Am. Chem. Soc.* **2004**, *126*, 10854–10855.
- Chen, J. Y.; Xiong, Y. J.; Yin, Y. D.; Xia, Y. N. Pt Nanoparticles Surfactant-Directed Assembled into Colloidal Spheres and Used as Substrates in Forming Pt Nanorods and Nanowires. *Small* **2006**, *2*, 1340–1343.
- Lee, E. P.; Chen, J.; Yin, Y.; Campbell, C. T.; Xia, Y. Pd-Catalyzed Growth of Pt Nanoparticles or Nanowires as Dense Coatings on Polymeric and Ceramic Particulate Supports. *Adv. Mater.* **2006**, *18*, 3271–3274.
- Lee, E. P.; Peng, Z.; Cate, D. M.; Yang, H.; Campbell, C. T.; Xia, Y. Growing Pt Nanowires as a Densely Packed Array on Metal Gauze. *J. Am. Chem. Soc.* **2007**, *129*, 10634–10635.
- Tian, N.; Zhou, Z. Y.; Sun, S. G.; Ding, Y.; Wang, Z. L. Synthesis of Tetrahedral Platinum Nanocrystals with High-Index Facets and High Electro-Oxidation Activity. *Science* **2007**, *316*, 732–735.
- Yamauchi, Y.; Sugiyama, A.; Morimoto, R.; Takai, A.; Kuroda, K. Mesoporous Platinum with Giant Mesocages Templated from Lyotropic Liquid Crystals Consisting of Diblock Copolymers. *Angew. Chem., Int. Ed.* **2008**, *47*, 5371–5373.
- Yamauchi, Y.; Takai, A.; Nagaura, T.; Inoue, S.; Kuroda, K. Pt Fibers with Stacked Donut-like Mesospace by Assembling Pt Nanoparticles: Guided Deposition in Physically Confined Self-Assembly of Surfactants. *J. Am. Chem. Soc.* **2008**, *130*, 5426–5427.
- Takai, A.; Yamauchi, Y.; Kuroda, K. Fabrication of Mesoporous Pt Nanotubes Utilizing Dual Templates under a Reduced Pressure Condition. *Chem. Commun.* **2008**, 4171–4173.
- Yamauchi, Y.; Takai, A.; Komatsu, M.; Sawada, M.; Ohsuna, T.; Kuroda, K. Vapor Infiltration of a Reducing Agent for Facile Synthesis of Mesoporous Pt and Pt-Based Alloys and Its Application for the Preparation of Mesoporous Pt Microrods in Anodic Porous Membranes. *Chem. Mater.* **2008**, *20*, 1004–1011.
- Mahmoud, M. A.; Tabor, C. E.; Ding, Y.; Wang, Z. L.; El-Sayed, M. A. A New Catalytically Active Colloidal Platinum Nanocatalyst: The Multiarmed NanoStar Single Crystal. *J. Am. Chem. Soc.* **2008**, *130*, 4590–4591.
- Peng, Z.; Yang, H. Synthesis and Oxygen Reduction Electrocatalytic Property of Pt-on-Pd Bimetallic Heteronanostructures. *J. Am. Chem. Soc.* **2009**, *131*, 7542–7543.
- Wang, L.; Yamauchi, Y. Block Copolymer Mediated Synthesis of Dendritic Platinum Nanoparticles. *J. Am. Chem. Soc.* **2009**, *131*, 9152–9153.
- Lim, B.; Jiang, M.; Camargo, P. H. C.; Cho, E. C.; Tao, J.; Lu, X.; Zhu, Y.; Xia, Y. Pd–Pt Bimetallic Nanodendrites with High Activity for Oxygen Reduction. *Science* **2009**, *324*, 1302–1305.

21. Jasuja, K.; Berry, V. Implantation and Growth of Dendritic Gold Nanostructures on Graphene Derivatives: Electrical Property Tailoring and Raman Enhancement. *ACS Nano* **2009**, *3*, 2358–2366.
22. Geim, A. K.; Novoselov, K. S. The Rise of Graphene. *Nat. Mater.* **2007**, *6*, 183–191.
23. Bunch, J. S.; Van Der Zande, A. M.; Verbridge, S. S.; Frank, I. W.; Tanenbaum, D. M.; Parpia, J. M.; Craighead, H. G.; McEuen, P. L. Electromechanical Resonators from Graphene Sheets. *Science* **2007**, *315*, 490–493.
24. Park, S.; Ruoff, R. S. Chemical Methods for the Production of Graphenes. *Nat. Nanotechnol.* **2009**, *4*, 217–224.
25. Yoo, E.; Okata, T.; Akita, T.; Kohyama, M.; Nakamura, J.; Honma, I. Enhanced Electrocatalytic Activity of Pt Subnanoclusters on Graphene Nanosheet Surface. *Nano Lett.* **2009**, *9*, 2255–2259.
26. Li, Y. M.; Tang, L. H.; Li, J. H. Preparation and Electrochemical Performance for Methanol Oxidation of Pt/Graphene Nanocomposites. *Electrochem. Commun.* **2009**, *11*, 846–849.
27. Seger, B.; Kamat, P. V. Electrocatalytically Active Graphene–Platinum Nanocomposites. Role of 2-D Carbon Support in PEM Fuel Cells. *J. Phys. Chem. C* **2009**, *113*, 7990–7995.
28. Guo, S. J.; Fang, Y. X.; Dong, S. J.; Wang, E. K. High-Efficiency and Low-Cost Hybrid Nanomaterial as Enhancing Electrocatalyst: Spongelike Au/Pt Core/Shell Nanomaterial with Hollow Cavity. *J. Phys. Chem. C* **2007**, *111*, 17104–17109.
29. Guo, S. J.; Wang, L.; Dong, S. J.; Wang, E. K. A Novel Urchinlike Gold/Platinum Hybrid Nanocatalyst with Controlled Size. *J. Phys. Chem. C* **2008**, *112*, 13510.
30. Guo, S. J.; Dong, S. J.; Wang, E. K. Raspberry-like Hierarchical Au/Pt Nanoparticle Assembling Hollow Spheres with Nanochannels: An Advanced Nanoelectrocatalyst for the Oxygen Reduction Reaction. *J. Phys. Chem. C* **2009**, *113*, 5485.
31. Guo, S. J.; Dong, S. J.; Wang, E. K. Gold/Platinum Hybrid Nanoparticles Supported on Multiwalled Carbon Nanotube/Silica Coaxial Nanocables: Preparation and Application as Electrocatalysts for Oxygen Reduction. *J. Phys. Chem. C* **2008**, *112*, 2389.
32. Wang, S. Y.; Kristian, N.; Jiang, S. P.; Wang, X. Controlled Synthesis of Dendritic Au@Pt Core–Shell Nanomaterials for Use as an Effective Fuel Cell Electrocatalyst. *Nanotechnology* **2009**, *20*, 025605.
33. Wang, S. Y.; Kristian, N.; Jiang, S. P.; Wang, X. Controlled Deposition of Pt on Au Nanorods and Their Catalytic Activity towards Formic Acid Oxidation. *Electrochem. Commun.* **2008**, *10*, 961–964.
34. Wang, S. Y.; Wang, X.; Jiang, S. P. PtRu Nanoparticles Supported on 1-Aminopyrene-Functionalized Multiwalled Carbon Nanotubes and Their Electrocatalytic Activity for Methanol Oxidation. *Langmuir* **2008**, *24*, 10505–10512.
35. Guo, S. J.; Huang, L. J.; Wang, E. K. A Novel Hybrid Nanostructure Based on SiO₂@Carbon Nanotube Coaxial Nanocable. *New J. Chem.* **2007**, *31*, 575–579.
36. Li, D.; Müller, M. B.; Gilje, S.; Kaner, R. B.; Wallace, G. G. Processable Aqueous Dispersions of Graphene Nanosheets. *Nat. Nanotechnol.* **2008**, *3*, 101–105.
37. Stankovich, S.; Dikin, D. A.; Piner, R. D.; Kohlhaas, K. A.; Kleinhammes, A.; Jia, Y.; Wu, Y.; Nguyen, S. T.; Ruoff, R. S. Synthesis of Graphene-Based Nanosheets via Chemical Reduction of Exfoliated Graphite Oxide. *Carbon* **2007**, *45*, 1558–1565.
38. Tung, V. C.; Allen, M. J.; Yang, Y.; Kaner, R. B. High-Throughput Solution Processing of Large-Scale Graphene. *Nat. Nanotechnol.* **2009**, *4*, 25.
39. Wu, B.; Hu, D.; Kuang, Y.; Liu, B.; Zhang, X.; Chen, J. Functionalization of Carbon Nanotubes by an Ionic-Liquid Polymer: Dispersion of Pt and PtRu Nanoparticles on Carbon Nanotubes and Their Electrocatalytic Oxidation of Methanol. *Angew. Chem., Int. Ed.* **2009**, *48*, 4751–4754.
40. Hsin, Y. L.; Hwang, K. C.; Yeh, C.-T. Poly(vinylpyrrolidone)-Modified Graphite Carbon Nanofibers as Promising Supports for PtRu Catalysts in Direct Methanol Fuel Cells. *J. Am. Chem. Soc.* **2007**, *129*, 9999–10010.
41. Mu, Y.; Liang, H.; Hu, J.; Jiang, L.; Wan, L. Controllable Pt Nanoparticle Deposition on Carbon Nanotubes as an Anode Catalyst for Direct Methanol Fuel Cells. *J. Phys. Chem. B* **2005**, *109*, 22212–22216.
42. Zheng, S.-F.; Hu, J.-S.; Zhong, L.-S.; Wan, L.-J.; Song, W.-G. *In Situ* One-Step Method for Preparing Carbon Nanotubes and Pt Composite Catalysts and Their Performance for Methanol Oxidation. *J. Phys. Chem. C* **2007**, *111*, 11174–11179.
43. Guo, S. J.; Dong, S. J.; Wang, E. K. Polyaniline/Pt Hybrid Nanofibers: High-Efficiency Nanoelectrocatalysts for Electrochemical Devices. *Small* **2009**, *5*, 1869–1876.